

# EFormer: Enhanced Transformer towards Semantic-Contour Features of Foreground for Portraits Matting

Zitao Wang, Qiguang Miao, Yue Xi

Paper ID \*\*\*

**Abstract.** The portrait matting task aims to extract an alpha matte with complete semantics and finely-detailed contours. In comparison to CNN-based approaches, transformers with self-attention allow a larger receptive field, enabling it to better capture long-range dependencies and low-frequency semantic information of a portrait. However, the recent research shows that self-attention mechanism struggle with modeling high-frequency information and capturing fine contour details, which can lead to bias while predicting the portrait’s contours. To address the problem, we propose EFormer to enhance the model’s attention towards semantic and contour features. Especially the latter, which is surrounded by a large amount of high-frequency details. We build a semantic and contour detector (SCD) to accurately capture the distribution of semantic and contour features. And we further design contour-edge extraction branch and semantic extraction branch for refining contour features and complete semantic information. Finally, we fuse the two kinds of features and leverage the segmentation head to generate the predicted portrait matte. Remarkably, EFormer is an end-to-end trimap-free method and boasts a simple structure. Experiments conducted on VideoMatte240K-JPEGSD and AIM datasets demonstrate that EFormer outperforms previous portrait matte methods.

## 1 Introduction

Portrait matting aims to extract the precise alpha matte of persons from natural images. It has gathered great momentum in vision applications, including but not limited to photo editing and background replacement.

Existing methods[1,2,3,4] attempt to estimate a portrait matte with Convolutional Neural Networks (CNNs) under the guidance of a pre-determined trimap, which is a three-class map that indicates the foreground, background, and unknown region. However, it is time-consuming and labor-intensive to obtain abundant their trimaps by manually annotate images.

Some methods eliminate the trimap, such as background matting series[5,6] uses a separate background image instead of the trimap as auxiliary reference for model prediction. However, in practical cases, it is necessary to provide two aligned images for the model, which include one with only the background and

the other one including people. An alternative solution[6,7,8,9] is to rely solely on RGB images as input for predicting portrait mattes.

Although the previous model has made strides in portrait matte, there is a constraint on the receptive field in CNN-based approaches. That means it is difficult to capture the global characteristics of an image.

Recently, Vision Transformer (ViT) for semantic segmentation [10,11] have employed a self-attention mechanism, which conducts interactions among all pixels in an image to obtain a global receptive field. ViT models [12] can capture the low-frequency components in images effectively, such as global shapes and structures of a scene or object. However, they usually neglect high-frequency ones in images, such as edges and textures. Inception Transformer (IFormer)[13] has revealed that ViT works similarly to low-pass filters.

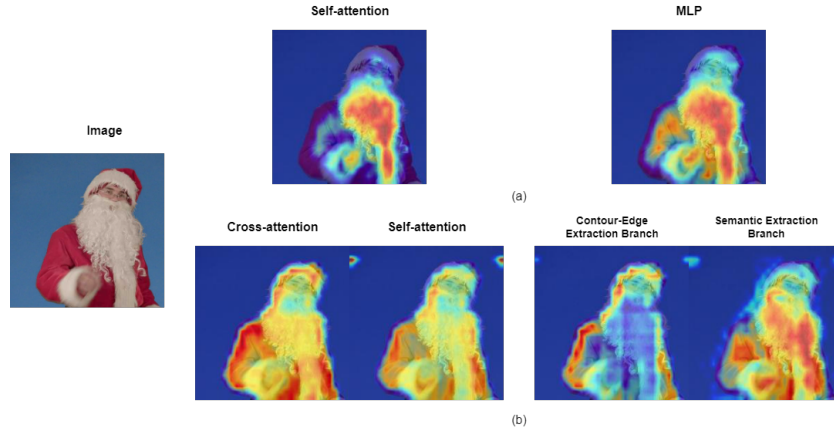


**Fig. 1.** We used Grad-CAM to visualize and compare the features learned by each layer within the transformer block. In Figure (a), we can observe the features capturing from self-attention and MLP layers in the original transformer block, which clearly have a low level of attention to the contour edges of the portrait. Moving onto Figure (b), after cross-attention at different resolutions in our transformer block, the attention to the contour edges becomes significantly more prominent. Figure (b) also shows the results of separating and extracting contour and semantic information from the two branches.

We believe that this phenomenon is due to the excessive propagation of global information. During the iterative process of multiple transformer blocks, each block performs a global attention. This calculation propagates global information throughout the model, ultimately leading it to focus on low-frequency semantic features within portraits. However, due to the difference between the local high-frequency features around the contours and the foreground low-frequency semantic features, the model gradually ignores the local high-frequency features.

Therefore, it is desired to capture low- and high-frequency components simultaneously to improve the segmentation performance.

IFormer splits all channels into convolutional path and self-attention path, respectively, to capture high and low frequencies. It is required for a channel ratio of each block at different levels in IFormer. These channel ratios typically require manual adjustment, resulting in significant uncertainty when aiming for optimal model performance. Therefore, it is desirable to design a novel ViT architecture, which can capture both high- and low-frequency components.

To tackle this issue, we propose a novel transformer block with the cross-attention on different resolution features, instead of convolution to handle high-frequency detail features. It can help model formulate more reasonable attention allocation mechanism to efficiently capture all frequency components.

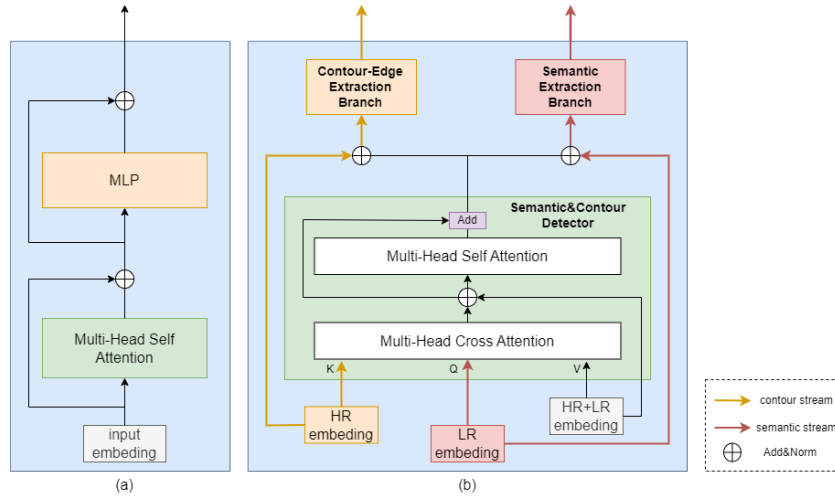


**Fig. 2.** Comparisons of different transformer blocks. (a) The original transformer block in ViT. (b) The proposed transformer block for portrait matte. Our transformer block cascades cross-attention between features with different resolutions and self-attention to sequentially extract objects’ contours and semantic features.

Our research demonstrates that the cross-attention between different resolutions can accurately capture the distribution of semantic and contour features. Particularly, our model with cross-attention can successfully capture the high-frequency details around the portrait’s contours, which are previously ignored by self-attention, as shown in Fig. 1.

It is worth noting that high-frequency components in the boundary between foreground and background are critical to the improvement of segmentation performance, rather than those inside foreground or background. Therefore, we follow a coarse-to-fine manner, first locate all high-frequency regions in the im-

age, and then filter the high-frequency regions along the edge of the foreground contours, with the semantic information of the foreground.

To achieve the above goals, we design a semantic and contour detector, which cascades cross-attention and self-attention to sequentially locate the contour and semantic features. Firstly, the model adjusts its attention on contour features with the guidance of cross-attention. Secondly, self-attention captures semantic information within a portrait’s contours, while reverse filtering and correcting the contour information output by cross-attention. This allows the model to gradually capture and match the contour information and the foreground semantic information.

Then, we use MLP to build the contour edge extraction branch and the semantic extraction branch, respectively. With this support, we independently purify the contour stream and the semantic stream to obtain finer contour information and more comprehensive portrait semantic information, as shown in Fig. 1(b).

Finally, in the prediction stage, we fuse the contour features and semantic features, and then send them to the segmentation head to estimate portrait matte.

We have performed extensive experiments on VideoMatte240K-JPEGSD[6], AIM[4], and BG10K. Comparisons with other state-of-the-art models and ablation studies verify that our model performs better than previous works.

To summarize, our contributions are as follows:

- We have presented a novel network architecture: EFormer, which can enhance the transformer’s attention towards both semantic and contour features of foreground.
- We further build a semantic and contour detector (SCD) to accurately capture the distribution of semantic and contour features and design two separate extraction branches to improve the performance of EFormer on portrait matting.
- Remarkably, our network is the first to leverage cross-attention between different resolution features in the transformer block to autonomously capture and extract high-frequency detailed features that are sparsely distributed along the foreground contour. We hope that our work inspires the research community to explore further advances in this field.

## 2 Related Works

### 2.1 Image Matting

Image matting is an essential task in the field of computer vision that aims to accurately estimate the foreground in an image. Mathematically speaking, an image  $I$  is a combination of an unknown foreground image  $F$  and a background image  $B$  with a probability coefficient  $\alpha$  matte maps  $\alpha$ .

$$I = \alpha F + (1 - \alpha) B \tag{1}$$

Previous image matting solutions have predominantly focused on low-level features, such as color cues[14,15,16,17] or propagation[18,19,20], to distinguish

the transition areas between foregrounds and backgrounds. However, such traditional matting algorithms commonly struggle to perform properly in complex scenes.

With the significant advancements made in deep learning, numerous methods based on convolutional neural networks (CNNs) have been proposed, leading to notable successes. Some approaches incorporate auxiliary trimap supervisions to enhance matting performance, while other methods leverage trimap-free solutions to estimate alpha mattes from image feature maps using an end-to-end segmentation network. In the background matting series, an auxiliary input of the background image is used for compute alpha matte. Furthermore, MODNet employs a self-supervised method to model sub-objective consistency.

Although prior work based on CNN kernels has improved the accuracy of image matting, the prediction of models are in the limited receptive field.

## 2.2 Vision Transformer

In the realm of computer vision, vision transformers have gained significant attention in recent times. ViT uses an initial transformer encoder for image classification. In addition, the backbone of Swin employs hierarchical local vision transformers. DETR[21] implements a complete transformer for detecting objects.

For pixel level prediction tasks, such as segmentation, the transformer demonstrates promising performance. SegFormer[22] and DPT[23] apply transformer as encoder to attain multi-scale feature maps of images. SETR[24] proposes a sequence-to-sequence method and uses pretrained ViT as its backbone without resolution reduction. All of these methods use transformers with self-attention mechanisms to capture long-term dependencies.

But recent studies[12,13] indicate that transformer with self-attention is capable of building complete contextual information through global interactions, "yet is incompetent in capturing high frequencies that predominantly convey local information" by [13].

Compared to self-attention, cross-attention has more potential to induce customized features. Max-Deeplab[25], MaskFormer[26,27] and SeMask[28] use query-based methods through cross-attention, which are inspired by DETR. They approach segmentation as a set prediction problem. U-Transformer[29] and EUT[30] modify the cross-attention in the original transformer to leverage the information from the encoder, allowing a fine spatial recovery in the decoder. The cross-resolution attention employed by RTFormer[31] enables the gathering of comprehensive contextual information for high-resolution features.

In this work, we propose a strategy that use of cross-attention between different resolutions guides the model to autonomously detect and capture high-frequency features, particularly those close to the portrait's contours. Contrary to IFormer[13], this method eliminates the need for predefined parameters to enhance the model's adaptive capabilities. This approach can significantly improve the model's performance in detecting contour details.

### 2.3 Refinement for Segmentation

Many prior studies on segmentation refinement depend on convolutional networks or MLPs that are designed specifically for this purpose.

Based on the coarse predictions of Mask R-CNN[32], PointRend[33] calculates confidence scores as the point-wise uncertainty measure. And then it focuses on the points with the higher uncertainty according to set hyperparameters. Finally, PointRend uses a shared MLP to refine the labels of the selected points. Although PointRend has implemented segmentation refinement to some extent, the model still requires manual adjustment of certain hyperparameters to assist in filtering uncertain points.

Transfuser[34] processes detected error-prone and incoherent regions with transformer, which are mostly strewn along object boundaries or in high-frequency regions. However, during this procedure, excessive focus was placed on the local details and correlations of error front and incoherent regions, without effectively associating the local features of the object with the overall semantic information.

In the field of portrait segmentation, refining the high-frequency details near the contour is crucial. Locating effective detail distribution areas requires information interaction between local details and global semantics. To address this, we have designed a semantic and contour detector that adopts a cascade structure of cross attention and self-attention. This approach uses global semantic information garnered from self-attention to autonomously select out local details situated at the borders of the contours. On this basis, we further utilize the MLP-based extraction branch to purify contour details, thereby significantly enhancing the refinement effect.

## 3 Model

In this section, we will introduce the process of establishing the complete model architecture of EFormer, which comprises backbone for encoder, transformer block for decoder and the prediction stage, as shown in Fig. 3.

### 3.1 Backbone for Encoder

The backbone network takes RGB images as input to obtain 1/4, 1/8, and 1/16 downsampled features, which are denoted as  $F_{enc\frac{1}{4}}$ ,  $F_{enc\frac{1}{8}}$ , and  $F_{enc\frac{1}{16}}$ . The 1/8 feature represents  $F_{HR}$  (high resolution features), while the 1/16 feature represents  $F_{LR}$  (low resolution features).

$$F_{HR} = F_{enc\frac{1}{8}} \quad (2)$$

$$F_{LR} = F_{enc\frac{1}{16}} \quad (3)$$

We first perform a  $2\times$  upsampling operation on  $F_{LR}$ , and then use bottleneck to adjust the channels of  $F_{HR}$  and  $F_{LR}$  respectively. So that, the feature matrices

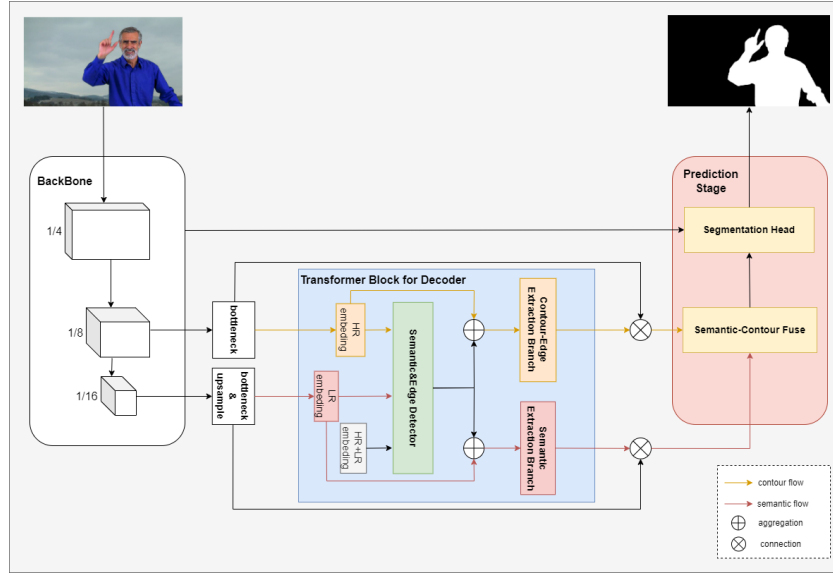


**Fig. 3.** The Architecture of the EFormer. It contains backbone for encoder, transformer block for decoder and the prediction stage, where transformer block includes a semantic and contour detector, a semantic extraction branch, and a contour-edge extraction branch.

of  $F'_{LR}$  and  $F'_{HR}$  have the same shape, where  $F'_{LR} \in R^{B \times C \times H \times W}$ ,  $F'_{HR} \in R^{B \times C \times H \times W}$ .

$$F'_{LR} = bottleneck(Upsample(F_{LR})) \tag{4}$$

$$F'_{HR} = bottleneck(F_{HR}) \tag{5}$$

Both of them will be utilized as inputs for the transformer block.

### 3.2 Transformer Block for Decoder

The decoder transformer is built using N consecutive blocks. Each transformer block, as shown in Fig. 4, includes a Semantic and Contour Detector (SCD), a Semantic Extraction Branch (SEB), and a Contour-Edge Extraction Branch (CEEB). The SCD consists of a cross-attention layer (CA) and a self-attention layer (SA). On the other hand, each of SEB and CEEB contains a multi-layer perceptron (MLP). To maintain consistency, Layer Norm (LN) is implemented in the input of the CA, SA, SEB, and CEEB. Additionally, a residual connection is applied to the output of CA, SA, SEB, and CEEB. Absolute and learnable position encoding (PE) is used in the transformer block.

**Semantic and Contour Detector (SCD)** This detector is optimized to effectively allocate attention to both the high-frequency detail features along the

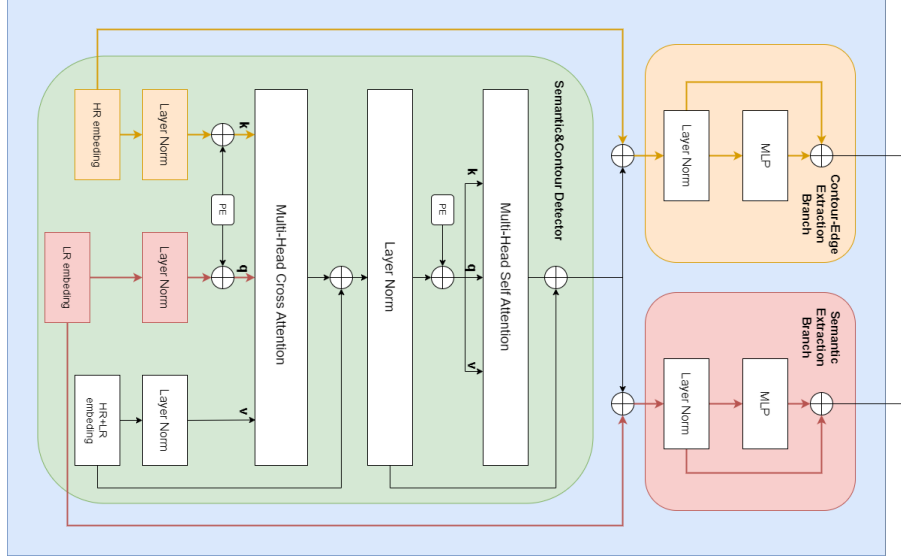


**Fig. 4.** Our transformer block includes a Semantic and Contour Detector (SCD), a Semantic Extraction Branch (SEB), and a Contour-Edge Extraction Branch (CEEB). The detailed composition of the model is shown in the figure.

contours of the portrait and the low-frequency semantic features within the portrait. This ensures an outcome that is optimal for both types of features. To achieve this, we sequentially use a cross-attention layer (CA) and a self-attention layer (SA) within the detector. We get  $F_{HR}^{em}$  and  $F_{LR}^{em}$  through flatten operation:

$$F_{HR}^{em} = Flatten(F'_{HR}) \quad (6)$$

$$F_{LR}^{em} = Flatten(F'_{LR}) \quad (7)$$

where  $F_{LR}^{em} \in R^{N \times B \times C}$ ,  $F_{HR}^{em} \in R^{N \times B \times C}$ , and  $N = H \times W$ . The input  $K, Q, V$  of the cross-attention layer (CA) is calculated as

$$K = LN(F_{HR}^{em}) + PE \quad (8)$$

$$Q = LN(F_{LR}^{em}) + PE \quad (9)$$

$$V = LN(F_{LR}^{em} + F_{HR}^{em}) \quad (10)$$

By performing cross-attention calculations using features of varying resolutions, it is possible to automatically detect the discrete distribution of contours along the portrait and allocate more attention to corresponding positions. The contour-edge features can be derived from the output of the CA.

$$F_{contour-edge} = CA(K, Q, V) \quad (11)$$

While CA pays extra attention to contour-edge features, it still captures the overall semantic. By the residual connection between CA and  $V$ , both the semantic

and contour-edge features of the portrait are enhanced, especially contour-edge features.

$$F_{enhance} = CA(K, Q, V) + V \quad (12)$$

Since semantic information is still present, we use the  $F_{enhance}$  as input of the self-attention layer (SA) to detect the distribution of semantic feature, thereby emphasizing the semantic attributes at their respective positions.

$$F'_{enhance} = LN(F_{enhance}) \quad (13)$$

After using LN to normalize  $F_{enhance}$ , the input  $K'$ ,  $Q'$ ,  $V'$  of the SA is calculated as

$$K' = Q' = F'_{enhance} + PE \quad (14)$$

$$V' = F'_{enhance} \quad (15)$$

Through SA filtering the semantic and contour features and residual connection between  $V'$  and the output of SA, we can produce  $F_{semantic-contour}$  as the output of the semantic and contour detector.

$$F_{semantic-contour} = SA(K', Q', V') + V' \quad (16)$$

**Contour-Edge Extraction Branch (CEEB)** In order to further capture and refine high-frequency contour details we construct this branch, which aggregates  $F_{semantic-contour}$  and  $F_{HR}^{em}$ , normalizes the results by LN, and uses MLP to extract contour edge features individually.

$$F_{contour} = MLP(LN(F_{HR}^{em} + F_{semantic-contour})) \quad (17)$$

**Semantic Extraction Branch (SEB)** Similarly, to obtain more comprehensive and consistent portrait semantic features by this branch, we merge  $F_{semantic-contour}$  and  $F_{LR}^{em}$ , normalize the outcomes applying LN, and employ MLP to extract portrait semantic features separately.

$$F_{semantic} = MLP(LN(F_{LR}^{em} + F_{semantic-contour})) \quad (18)$$

### 3.3 Prediction Stage

After getting key characteristics  $F_{semantic} \in R^{N \times B \times C}$  and  $F_{contour} \in R^{N \times B \times C}$  from transformer block, where  $N = H \times W$ , we transform them into  $F'_{semantic} \in R^{B \times C \times H \times W}$  and  $F'_{contour} \in R^{B \times C \times H \times W}$  by converting the vector into the matrix. To achieve improved outcomes in portrait segmentation, we propose fusing the two kinds of features and ultimately acquiring the predicted portrait matte from the segmentation head module.

**Fuse** We attain the semantic feature through residual connection between  $F'_{LR}$  and  $F'_{semantic}$  of semantic flow. Similarly, we get contour feature from contour flow and subsequently merge the  $F'_{semantic}$  and  $F'_{contour}$  to generate the fused features  $F_{semantic-contour-fuse}$ .

$$F'_{semantic} = Conv(F'_{semantic} + F'_{LR}) \quad (19)$$

$$F'_{contour} = Conv(F'_{contour} + F'_{HR}) \quad (20)$$

$$F_{semantic-contour-fuse} = Upsample(Conv(F'_{semantic} + F'_{contour})) \quad (21)$$

### Segmentation Head

$$matte = Upsample\left(Conv\left(F_{semantic-contour-fuse} + F_{enc\frac{1}{4}}\right)\right) \quad (22)$$

Finally, We gather  $F_{semantic-contour-fuse}$  and  $F_{enc\frac{1}{4}}$  with higher resolution to predicted portrait matte in 1/4 scale of the input image and upscale it to the original scale through bi-linear interpolation as the output of our model.

**Loss function** To compute losses during the training stage, we use a Binary CrossEntropy Loss function.

$$L_{bce} = -(g(x, y) \times \log(p(x, y)) + (1 - g(x, y)) \times \log(1 - p(x, y))) \quad (23)$$

Where,  $p(x, y)$  is prediction of network,  $g(x, y)$  is ground truth.

## 4 Experiments

### 4.1 Dataset and Evaluation

**Dataset** We utilize composite training data from two sources: the foreground image dataset VideoMatte240K-JPEGSD[6] and AIM[4]. For the background images, we selected BG10K following the approach of BGMv2[6], which is a collection of photographs depicting various life scenes without any human portraits. We select foregrounds from VideoMatte240K-JPEGSD and AIM, backgrounds from BG10K to composite image datasets. We split VideoMatte240K-JPEGSD into 234,982/3,007/2720 image sets with image resolutions of  $224 \times 224$  and  $512 \times 288$  for training, validating, and testing our model. Similarly, BG10K is split into 9000/1000 image sets, and AIM is split into 214/10 image sets for training and testing, where AIM only includes the portrait images with resolutions at  $512 \times 512$ . Finally, we use the aforementioned testing datasets to compare and evaluate the performance of EFormer against other models.

**Evaluation** We mainly consider portrait matting accuracy for evaluation. For portrait matting accuracy, we use Mean Absolute Difference (MAD), Mean Squared Error (MSE), Gradient (Grad), and Connectivity (Conn) as evaluation metrics. We also scale MAD, MSE, Grad, and Conn by  $10^3$ ,  $10^3$ ,  $10^{-3}$ , and  $10^{-3}$  respectively, for convenience of reference. For all these metrics, the lower number represents better performance.

## 4.2 Implementation Details

**Training Settings** For training the network, we use a single RTX 3090 GPU with batch size at 24. The optimizer is AdamW and the initial learning rate is set to  $10^{-4}$ . All models in ablation studies are trained for 25 epochs, with the learning rate decaying by a factor of 0.8 every 5 epochs. Additionally, to augment the data, each input image is subjected to random horizontal flipping.

**Backbone** The backbone we use for the network is the pretrained ResNet50[35], since it is the most frequently used backbone in prior works. We use the implementation and weights from torchvision.

**Transformer Block for Decoder** The transformer block is based on the transformer encoder of DETR. We continuously use four transformer blocks in the decoder of the network. We set the channel  $C = 256$  and the number of attention heads  $M = 8$  for each multi-head attention module.

**Prediction Stage** After obtaining the semantic and contour feature maps of the portrait from the stacked transformer blocks, we fuse both of them. Then, the alpha mattes predicted by the segmentation head are upsampled to the original size of the input image with bilinear interpolation.

## 4.3 Ablation Studies

**Training Epochs** In the ablation study with an image resolution of  $224 \times 224$ , we conducted 25 training epochs. Every 5 epochs of training, we evaluated the training effect of the model, at the same time, the Learning rate reduced by 0.8 times. The experimental results indicate that our model achieved optimal performance in the 20 epoch, as shown in the Table 1.

**Table 1.** Ablation Study on the Training Epochs (resolution at  $224 \times 224$ ). **Bold** indicates the best performance among these models. We use the result of 20-epoch training as a strong baseline model.

	MAD↓	MSE↓	Grad↓	Conn↓
5-epoch	4.3953	1.4824	0.4089	0.1865
10-epoch	4.3108	1.4766	0.3908	0.1834
15-epoch	4.2867	1.5238	0.4087	0.1833
20-epoch	<b>4.1357</b>	<b>1.4280</b>	<b>0.3760</b>	<b>0.1753</b>
25-epoch	4.1811	1.4797	0.3858	0.1779

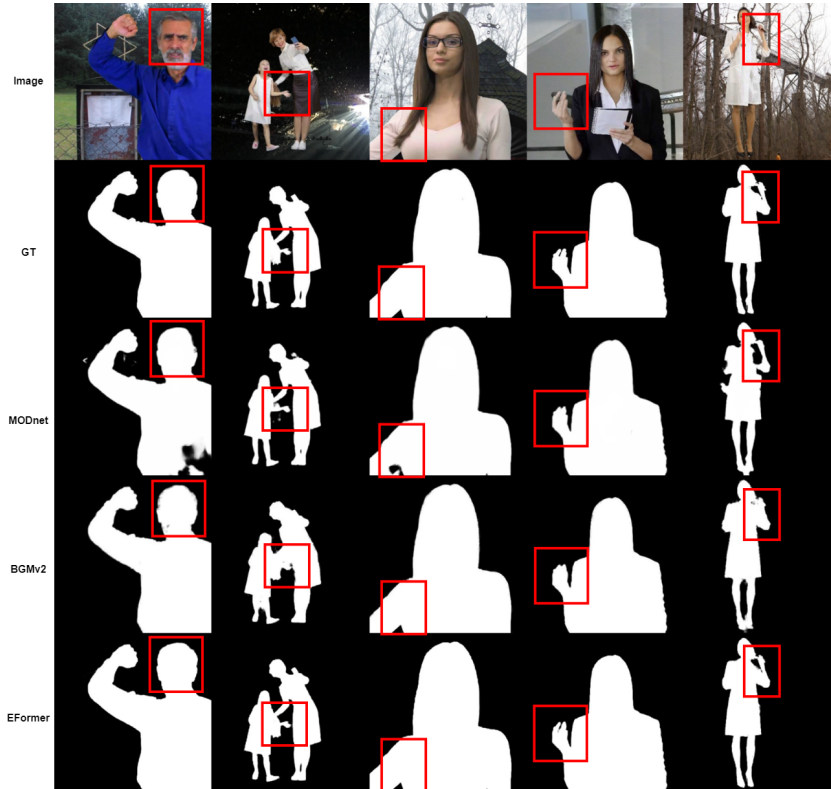


**Fig. 5.** Visualization of portrait matte predictions from MODnet, BGMv2, and EFormer under challenging image from the test set of VideoMatte240K-JPEGSD. Our model shows a better ability to distinguish ambiguous foreground contours, as indicated by the red box. Please zoom in to view the detailed information.

**The Functional Role of Each Module** To demonstrate the effectiveness of the model in detecting and extracting contour details and portrait semantics, we analyzed the outputs of CA, SA, CEEB, and SEB, and utilized Class Activation Map (CAM) to visualize the attention allocation of each layer’s features, as shown in Fig. 6.

From the first line of Fig. 6, it can be evident that after the cross attention layer, the model clearly strengthens its attention to the contour edges of the portrait. Following the contour prior, self attention layer detects the portrait’s semantics thoroughly. CEEB and SEB models provide sharper contour edges and comprehensive semantic information.

Comparing the second and first lines of Fig. 6, it is observed that removing the self attention layer considerably weakens the semantic information extracted by SEB.

In the comparison between the third and first lines of Fig. 6, it can be indicated that removing the cross attention layer significantly weakens the contour edge information extracted by CEEB.

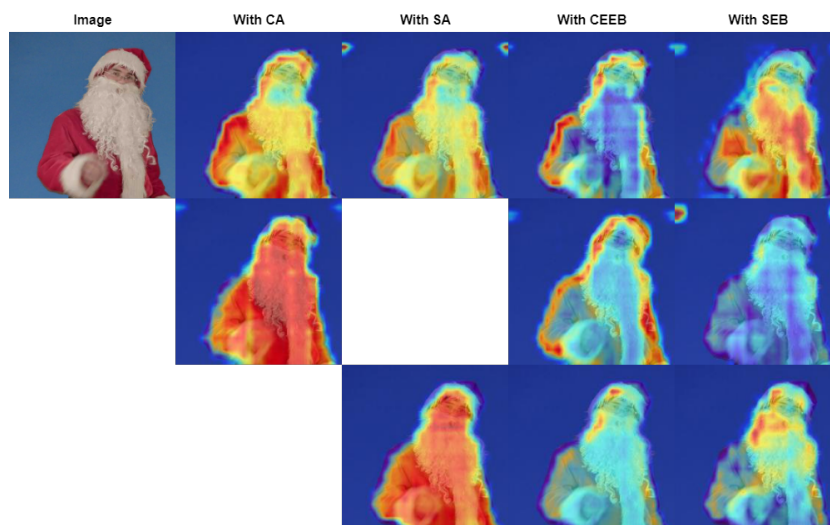


**Fig. 6.** We use Grad-CAM to visualize the attention distribution of various features in CA, SA, CEEB, and SEB. The model in the first row contains four complete modules. For comparison, the SA layer and CA layer were removed from the models in the second and third rows, respectively.

After qualitative analysis, the prediction results of all the above models were evaluated. It is concluding that the model with CA, SA, CEEB, and SEB is both effective and rational, as demonstrated in the Table 2.

As is well known, when it comes to extracting features for portrait segmentation tasks, semantic information plays a significant role, in contrast, contour

**Table 2.** Ablation Study on the Functional Role of CA and SA (resolution at  $224 \times 224$ ). **Bold** indicates the best performance among these models.

CA	SA	MAD↓	MSE↓	Grad↓	Conn↓
✓		4.2762	1.5344	0.4092	0.1823
	✓	4.1710	1.4354	0.3773	0.1769
✓	✓	<b>4.1357</b>	<b>1.4280</b>	<b>0.3760</b>	<b>0.1753</b>

details account for a relatively small proportion. Owing to this, , as shown in the Table 2 and Fig. 6, the absence of SA leads to a significant increase in all metrics due to the lack of amount of semantic information, while the model without CA experienced a slight increase in all indicators due to the loss of contour details. In order to fully harness the potential of the vision transformer, we integrate both CA and SA to ensure semantic completeness and enhance attention towards contour details, thereby achieving more comprehensive and fine-grained segmentation results.

#### 4.4 Comparisons to State-of-the-art Methods

To demonstrate the progressiveness of EFormer, we will compare it against the latest state-of-the-art trimap-free portrait matting solutions. These are including DeepLabV3[36] with ResNet101[35] backbone, BGMv2[6] with MobileNetV2[37] backbone, MODNet[7], and RVM[8]. Our assessment will be based on the testing datasets of VideoMatte240K-JPEGSD and AIM, respectively. As the training files for MODNet are not available, we will use its official weights. Furthermore, since BGMv2, DeepLabV3, and RVM have already been trained on all datasets, our method can be compared with them in a fair manner.

As shown in the Table 3 and the Table 4, our model exhibits superior performance in portrait matte tasks. It has a stronger capability to distinguish the contour of a portrait and can finely segment edge details (e.g. fingers), as exemplified in Fig. 5.

**Table 3.** Comparisons on the test set of VideoMatte240K-JPEGSD. **Bold** indicates the best performance among these models under the inputs with the same resolution at  $512 \times 288$ .

Model	MAD↓	MSE↓	Grad↓	Conn↓
DeepLabv3[36]	14.4700	9.6700	8.5500	1.6900
MODnet[7]	10.3900	5.6500	2.0200	1.0400
BGMv2[6]	4.1858	1.7934	1.3011	0.5326
RVM[8]	5.9900	1.1700	1.1000	0.3400
EFormer	<b>2.3097</b>	<b>0.6637</b>	<b>0.4580</b>	<b>0.2740</b>

**Table 4.** Comparisons on the test set of AIM. **Bold** indicates the best performance among these models under the inputs with the same resolution at  $512 \times 512$ .

Model	MAD↓	MSE↓	Grad↓	Conn↓
DeepLabv3[36]	29.64	23.78	20.17	7.71
MODnet[7]	21.66	14.27	5.37	5.23
BGMv2[6]	44.61	39.08	5.54	11.60
RVM[8]	14.84	8.93	4.35	3.83
EFormer	<b>7.47</b>	<b>2.13</b>	<b>2.83</b>	<b>1.90</b>

## 5 Conclusion

In this paper, we propose EFormer, which can strengthen the transformer’s attention to semantic and contour features of foreground, improving the prediction accuracy of portrait matting. Our transformer block incorporates cross-attention and self-attention to establish a semantic and contour detector, which effectively guides the model to focus on both semantic and contours features, especially the latter. Additionally, we further build a contour edge extraction branch and a semantic extraction branch to capture finer details around the contour edge and more comprehensive portrait semantic information. Extensive experiments show that our method outperforms previous portrait matting solutions and exhibits robust performance during testing and inference.

## References

1. Li, Y., Lu, H.: Natural image matting via guided contextual attention. In: Proceedings of the AAAI Conference on Artificial Intelligence. Volume 34. (2020) 11450–11457
2. Sun, Y., Wang, G., Gu, Q., Tang, C.K., Tai, Y.W.: Deep video matting via spatio-temporal alignment and aggregation. In: Proceedings of the IEEE/CVF Conference on Computer Vision and Pattern Recognition. (2021) 6975–6984
3. Wang, Y., Niu, Y., Duan, P., Lin, J., Zheng, Y.: Deep propagation based image matting. In: IJCAI. Volume 3. (2018) 999–1006
4. Xu, N., Price, B., Cohen, S., Huang, T.: Deep image matting. In: Proceedings of the IEEE conference on computer vision and pattern recognition. (2017) 2970–2979
5. Sengupta, S., Jayaram, V., Curless, B., Seitz, S.M., Kemelmacher-Shlizerman, I.: Background matting: The world is your green screen. In: Proceedings of the IEEE/CVF Conference on Computer Vision and Pattern Recognition. (2020) 2291–2300
6. Lin, S., Ryabtsev, A., Sengupta, S., Curless, B.L., Seitz, S.M., Kemelmacher-Shlizerman, I.: Real-time high-resolution background matting. In: Proceedings of the IEEE/CVF Conference on Computer Vision and Pattern Recognition. (2021) 8762–8771

7. Ke, Z., Sun, J., Li, K., Yan, Q., Lau, R.W.: Modnet: Real-time trimap-free portrait matting via objective decomposition. In: Proceedings of the AAAI Conference on Artificial Intelligence. Volume 36. (2022) 1140–1147
8. Lin, S., Yang, L., Saleemi, I., Sengupta, S.: Robust high-resolution video matting with temporal guidance. In: Proceedings of the IEEE/CVF Winter Conference on Applications of Computer Vision. (2022) 238–247
9. Lin, T.Y., Goyal, P., Girshick, R., He, K., Dollár, P.: Focal loss for dense object detection. In: Proceedings of the IEEE international conference on computer vision. (2017) 2980–2988
10. Dosovitskiy, A., Beyer, L., Kolesnikov, A., Weissenborn, D., Zhai, X., Unterthiner, T., Dehghani, M., Minderer, M., Heigold, G., Gelly, S., et al.: An image is worth 16x16 words: Transformers for image recognition at scale. arXiv preprint arXiv:2010.11929 (2020)
11. Liu, Z., Lin, Y., Cao, Y., Hu, H., Wei, Y., Zhang, Z., Lin, S., Guo, B.: Swin transformer: Hierarchical vision transformer using shifted windows. In: Proceedings of the IEEE/CVF international conference on computer vision. (2021) 10012–10022
12. Park, N., Kim, S.: How do vision transformers work? arXiv preprint arXiv:2202.06709 (2022)
13. Si, C., Yu, W., Zhou, P., Zhou, Y., Wang, X., Yan, S.: Inception transformer. Advances in Neural Information Processing Systems **35** (2022) 23495–23509
14. Feng, X., Liang, X., Zhang, Z.: A cluster sampling method for image matting via sparse coding. In: Computer Vision–ECCV 2016: 14th European Conference, Amsterdam, The Netherlands, October 11–14, 2016, Proceedings, Part II 14, Springer (2016) 204–219
15. He, K., Rhemann, C., Rother, C., Tang, X., Sun, J.: A global sampling method for alpha matting. In: CVPR 2011, Ieee (2011) 2049–2056
16. Johnson, J., Varnousfaderani, E.S., Cholakkal, H., Rajan, D.: Sparse coding for alpha matting. IEEE Transactions on Image Processing **25** (2016) 3032–3043
17. Karacan, L., Erdem, A., Erdem, E.: Image matting with kl-divergence based sparse sampling. In: Proceedings of the IEEE international conference on computer vision. (2015) 424–432
18. Aksoy, Y., Oh, T.H., Paris, S., Pollefeys, M., Matusik, W.: Semantic soft segmentation. ACM Transactions on Graphics (TOG) **37** (2018) 1–13
19. Aksoy, Y., Ozan Aydin, T., Pollefeys, M.: Designing effective inter-pixel information flow for natural image matting. In: Proceedings of the IEEE Conference on Computer Vision and Pattern Recognition. (2017) 29–37
20. Levin, A., Rav-Acha, A., Lischinski, D.: Spectral matting. IEEE transactions on pattern analysis and machine intelligence **30** (2008) 1699–1712
21. Carion, N., Massa, F., Synnaeve, G., Usunier, N., Kirillov, A., Zagoruyko, S.: End-to-end object detection with transformers. In: European conference on computer vision, Springer (2020) 213–229
22. Xie, E., Wang, W., Yu, Z., Anandkumar, A., Alvarez, J.M., Luo, P.: Segformer: Simple and efficient design for semantic segmentation with transformers. Advances in Neural Information Processing Systems **34** (2021) 12077–12090
23. Ranftl, R., Bochkovskiy, A., Koltun, V.: Vision transformers for dense prediction. In: Proceedings of the IEEE/CVF international conference on computer vision. (2021) 12179–12188
24. Zheng, S., Lu, J., Zhao, H., Zhu, X., Luo, Z., Wang, Y., Fu, Y., Feng, J., Xiang, T., Torr, P.H., et al.: Rethinking semantic segmentation from a sequence-to-sequence perspective with transformers. In: Proceedings of the IEEE/CVF conference on computer vision and pattern recognition. (2021) 6881–6890

25. Wang, H., Zhu, Y., Adam, H., Yuille, A., Chen, L.C.: Max-deeplab: End-to-end panoptic segmentation with mask transformers. In: Proceedings of the IEEE/CVF conference on computer vision and pattern recognition. (2021) 5463–5474
26. Cheng, B., Misra, I., Schwing, A.G., Kirillov, A., Girdhar, R.: Masked-attention mask transformer for universal image segmentation. In: Proceedings of the IEEE/CVF conference on computer vision and pattern recognition. (2022) 1290–1299
27. Cheng, B., Schwing, A., Kirillov, A.: Per-pixel classification is not all you need for semantic segmentation. *Advances in Neural Information Processing Systems* **34** (2021) 17864–17875
28. Jain, J., Singh, A., Orlov, N., Huang, Z., Li, J., Walton, S., Shi, H.: Semask: Semantically masked transformers for semantic segmentation. *arXiv preprint arXiv:2112.12782* (2021)
29. Petit, O., Thome, N., Rambour, C., Themyr, L., Collins, T., Soler, L.: U-net transformer: Self and cross attention for medical image segmentation. In: *Machine Learning in Medical Imaging: 12th International Workshop, MLMI 2021, Held in Conjunction with MICCAI 2021, Strasbourg, France, September 27, 2021, Proceedings 12*, Springer (2021) 267–276
30. Du, D., Su, B., Li, Y., Qi, Z., Si, L., Shan, Y.: Efficient u-transformer with boundary-aware loss for action segmentation. *arXiv preprint arXiv:2205.13425* (2022)
31. Wang, J., Gou, C., Wu, Q., Feng, H., Han, J., Ding, E., Wang, J.: Rtformer: Efficient design for real-time semantic segmentation with transformer. *Advances in Neural Information Processing Systems* **35** (2022) 7423–7436
32. He, K., Gkioxari, G., Dollár, P., Girshick, R.: Mask r-cnn. In: Proceedings of the IEEE international conference on computer vision. (2017) 2961–2969
33. Kirillov, A., Wu, Y., He, K., Girshick, R.: Pointrend: Image segmentation as rendering. In: Proceedings of the IEEE/CVF conference on computer vision and pattern recognition. (2020) 9799–9808
34. Ke, L., Danelljan, M., Li, X., Tai, Y.W., Tang, C.K., Yu, F.: Mask transfiner for high-quality instance segmentation. In: Proceedings of the IEEE/CVF Conference on Computer Vision and Pattern Recognition. (2022) 4412–4421
35. He, K., Zhang, X., Ren, S., Sun, J.: Deep residual learning for image recognition. In: Proceedings of the IEEE conference on computer vision and pattern recognition. (2016) 770–778
36. Chen, L.C., Papandreou, G., Schroff, F., Adam, H.: Rethinking atrous convolution for semantic image segmentation. *arXiv preprint arXiv:1706.05587* (2017)
37. Sandler, M., Howard, A., Zhu, M., Zhmoginov, A., Chen, L.C.: Mobilenetv2: Inverted residuals and linear bottlenecks. In: Proceedings of the IEEE conference on computer vision and pattern recognition. (2018) 4510–4520